Astronomy & Astrophysics manuscript no. zeMainDraft
November 16, 2015
© ESO 2015

arXiv:1510.07600v2 [astro-ph.CO] 13 Nov 2015

Relieving tensions related to the lensing of CMB temperature power spectra

F. Couchot, S. Henrot-Versillé, O. Perdereau, S. Plaszczynski*, B. Rouillé d'Orfeuil, M. Spinelli and M. Tristram

Laboratoire de l'Accélérateur Linéaire, Univ. Paris-Sud, CNRS/IN2P3, Université Paris-Saclay, Orsay, France

Preprint online version: November 16, 2015

Abstract

The angular power spectra of the CMB temperature anisotropies reconstructed from *Planck* data seem to present 'too much' gravitational lensing distortion. This is quantified by the control parameter $A_{\rm L}$ that should be compatible with unity for a standard cosmology. Using the `class` Boltzmann solver and the profile likelihood method, we measure a 2.6σ discrepancy with 1 for the *Planck* public likelihoods. We show that, due to strong correlations with the reionization optical depth τ and the primordial perturbation amplitude $A_{\rm s}$, a $\sim 2\sigma$ tension on τ also appears between the low and high-ℓ likelihoods. With Hillipop, another high-ℓ likelihood built from *Planck* data, this difference is reduced to 1.3σ. In this case, the $A_{\rm L}$ value is still discrepant with 1 by 2.2σ, suggesting a non-trivial effect of the correlations between cosmological and nuisance parameters. To better constrain the foregrounds parameters, we include the very-high-ℓ measurements of the ACT and SPT experiments and finally obtain $A_{\rm L} = 1.03 \pm 0.08$. The Hillipop+ACT+SPT likelihood estimate of the optical depth is $\tau = 0.052 \pm 0.035$ which is fully compatible with the low-ℓ likelihood determination. After investigating the reasons for this improvement and showing the robustness of the results with various very-high-ℓ combinations, we provide estimates of the ΛCDM parameters with our regularized likelihood.

Key words. Cosmology: observations – Cosmology: theory – cosmic microwave background – cosmological parameters – Methods: statistical

1. Introduction

The $A_{\rm L}$ control parameter aims at measuring the degree of lensing of the CMB power spectra. From a set of cosmological parameters (Ω), a Boltzmann solver, such as `class` (Lesgourgues 2011a) or `camb` (Lewis et al. 2000), computes the angular power spectra of the temperature/polarization anisotropies $C_\ell(\Omega)$ and of the CMB lensing potential $C_\ell^\Phi(\Omega)$. The latter is then used to compute the distortion of the CMB spectra by the gravitational lensing (Blanchard & Schneider 1987), which redistributes the power across multipoles while preserving the brightness in a non-trivial way (e.g Lewis & Challinor 2006): $\{C_\ell(\Omega), C_\ell^\Phi(\Omega)\} \rightarrow \tilde{C}_\ell(\Omega)$. As originally proposed in Calabrese et al. (2008), a phenomenological parameter, $A_{\rm L}$, that re-scales the lensing potential, is introduced. This modifies the standard scheme into : $\{C_\ell(\Omega), A_{\rm L} \cdot C_\ell^\Phi(\Omega)\} \rightarrow \tilde{C}_\ell(\Omega, A_{\rm L})$. Sampling the likelihood, with this parameter left free, gives access to two interesting pieces of information:

1. from the $A_{\rm L}$ posterior distribution, one can check the consistency of the data with the model; it should be compatible with one for a standard cosmology.
2. by marginalizing over $A_{\rm L}$ one can study the impact of neglecting (to first-order) the lensing information contained in the CMB spectra.

Since its first release, the *Planck* Collaboration reports a value of the $A_{\rm L}$ parameter discrepant with one by more than 2σ. The full-mission result based on both a high and low-ℓ likelihood (Planck Collaboration XIII (2015), hereafter PCP15) is:

$$A_{\rm L} = 1.22 \pm 0.10 \quad (\textit{Planck}\ \text{TT+lowP}) \tag{1}$$

(all quoted errors are 68% CL intervals). As shown later, a profile likelihood analysis, as the one in Planck Collaboration Int. XVI (2014), rather points to a 2.6σ discrepancy.

This 'tension' may indicate a problem either on the model or the data side. The only solution for the model is to modify the computation of the geodesic deflection, i.e. to modify standard GR (Hu & Raveri 2015; Di Valentino et al. 2015). For the data, since *Planck* maps undergo a complicated treatment (for an overview see Planck Collaboration I 2015), one cannot exclude small residual systematic effects which could impact the details of the likelihood function in a different way from one implementation to the other.

The anomalously high $A_{\rm L}$ value directly affects the measurement of two ΛCDM parameters, the reionization optical depth τ and the primordial scalar perturbations amplitude $A_{\rm s}$. Indeed, in the high-ℓ regime, only the $\mathcal{A}_T \equiv A_{\rm s} e^{-2\tau}$ combination is constrained by the temperature power spectra amplitude. However this degeneracy is broken by the lensing distortion of the CMB anisotropies since $C_\ell^\Phi \propto A_{\rm s}$ (more perturbations induce more lensing) so that $A_{\rm s}$ and τ finally get both constrained.

The aim of this work is twofold. First, to clarify the connection between the $A_{\rm L}$ tension with unity and the one that also appears on τ between the *Planck* public high and low-ℓ likelihoods, and also to show that this effect may be related to the details of the nuisance parametrization in the likelihoods. By using Hillipop, a high-ℓ likelihood built from *Planck* data, and better constraining the astrophysical foregrounds and the high-ℓ part of the CMB spectrum with the high-angular resolution data from ACT and SPT, we show that one can obtain a more self-consistent picture of the ΛCDM parameters. Section 2 provides an in-depth discussion about $A_{\rm L}$ using the *Planck* baseline likelihoods, `Plik` and lowTEB, and make explicit the link with the determination of τ. Section 3 then recalls the main differences

*Corresponding author: <plaszczy@lal.in2p3.fr>

between Plik and Hillipop and discusses the first results with the latter. Then Sect. 4 describes how the inclusion of the ACT and SPT data was performed and, after various checks, discusses how their inclusion impacts the Hillipop results. Finally Sect. 5 discusses the results on the ΛCDM parameters using Hillipop in combination with other likelihoods.

2. The *Planck* A_L tension (and related parameters)

2.1. Planck likelihoods

Planck's baseline uses two different likelihood codes addressing different multipole ranges (see Planck Collaboration XI 2015, hereafter Like15):

1. the high-ℓ likelihood (Plik) is a Gaussian likelihood that acts in the multipole range $\ell \in [30, 2500]$. Data consist in a collection of angular power spectra that are derived from cross-correlated *Planck* 100, 143 and 217 GHz high frequency maps. For the results in this paper, we only use the temperature likelihood.
2. the low-ℓ likelihood (lowTEB) is a pixel-based likelihood relying essentially on the *Planck* low frequency instrument 70 GHz maps for polarization and on a component-separated map using all *Planck* frequencies for temperature. It acts in the $\ell \in [2, 29]$ range.

In the Like15 terminology, '*Planck* TT' refers to the combination of both the high and the low-ℓ temperature likelihoods. In this case, only the TT component of lowTEB is used. The '*Planck* TT+lowP' notation combines Plik to the full lowTEB likelihood which we will be labelled explicitly in this paper Plik+lowTEB.

In the following, we will make use of the publicly available Plik likelihood code (plik_dx11dr2_HM_v18_TT.clik)[1] with the Gaussian priors on nuisance parameters suggested by the *Planck* collaboration[2] where the information on foregrounds from the ACT and SPT data is propagated by a single SZ prior (PCP15, Sect. 2.3.1).

2.2. Boltzmann solver

The results derived in this paper make use of the Boltzmann equations solver class[3] while *Planck*'s published results were derived using camb[4]. Both softwares were compared previously (Lesgourgues 2011b) and produced spectra in excellent agreement when using their respective high precision settings. It was noticed more recently in PCP15 that sampling from any of them gives very compatible results on ΛCDM cosmological parameters. The precise estimate of the A_L parameter is more challenging since one deals with sub-percent effects on the spectra and requires further care about differences between both softwares.

For this purpose we sampled the Plik+lowTEB likelihoods in the ΛCDM+A_L model using class v2.4.3 and obtain results almost identical to the published ones. In particular we measure

$$A_L = 1.24 \pm 0.10 \quad \text{(Plik+lowTEB, class/MCMC)}, \qquad (2)$$

The tiny difference with respect to Eq. 1 can be traced down to a $O(1(\mu K)^2)$ difference on the high-ℓ part of the TT spectra (see Appendix A) but we consider that this general agreement is sufficient to perform reliable estimations. All further results will be derived consistently using class.

2.3. Profile likelihoods

In this paper, we will also often make use of a statistical methodology based on profile-likelihoods for reasons that will be clearer in Sect. 2.5. For a given parameter θ, we perform several multi-dimensional minimizations of the $\chi^2 \equiv -2 \ln \mathscr{L}$ function. Each time θ is fixed to a given $\theta(i)$ value, a minimization is performed with respect to all the other parameters, and the $\chi^2_{\rm min}(i)$ value is kept. The curve interpolated through the $\{\theta(i), \chi^2_{\rm min}(i)\}$ points and offset to 0, is known as the θ profile-likelihood: $\Delta\chi^2(\theta)$. We note that from the very construction procedure, the solution at the minimum of the profile always coincides with the complete 'best-fit' solution, i.e the Maximum Likelihood Estimate (MLE) of all the parameters. One obtains a genuine 68% CL interval by thresholding the profile at one even in non-Gaussian cases (e.g., James 2007).

This statistical method, alternative to MCMC, was discussed in Planck Collaboration Int. XVI (2014) and also used in Like15. Building a smooth profile from *Planck* data is computationally challenging since this approach requires an extreme precision on the $\chi^2_{\rm min}$ solution, typically better than 0.1 for values around 10^4. This goal can be achieved using the Minuit software[5] together with an increase of the class precision parameters. For the analysis presented in this paper, we have further refined the procedure described in Planck Collaboration Int. XVI (2014), as explained in Appendix B.

This procedure leads to a 'confidence interval' (e.g., James 2007). In the frequentist approach, it represents a statement on the data: when repeating the experiment many times, the probability for the reconstructed interval to cover the true value is 68%. The Bayesian approach, as implemented through a MCMC method, leads to what is generally referred to as a 'credible interval' derived from the probability density function of the true value. In most cases (in particular Gaussian) both intervals are very similar. However, in some cases (typically 'banana-shaped' 2D posteriors), those intervals may differ significantly (Porter 1996). In this case the mode (or mean) of the posterior distribution does not necessarily match the best fit solution and the existence of a difference between both values indicates what is referred to as 'likelihood volume effects'. In this paper, we will mainly focus on the details of the region around the maximum likelihood and thus will use consistently the profile-likelihood method.

2.4. A_L revisited

We first build the profile-likelihood for A_L (Fig. 1) and measure:

$$A_L = 1.26^{+0.11}_{-0.10} \quad \text{(Plik+lowTEB, class/profile)}. \qquad (3)$$

The shift with respect to Eq. 2 quantifies the size of the volume effects in the MCMC projection. It is of the same order of magnitude than the camb → class transition seen in Sect. 2.2. Using high-precision settings, we therefore find A_L at 2.6σ from 1.0.

[1] available in the Planck Legacy Archive (PLA): http://www.cosmos.esa.int/web/planck/pla

[2] http://wiki.cosmos.esa.int/planckpla2015/index.php/CMB_spectrum_&_Likelihood_Code

[3] http://class-code.net/

[4] http://camb.info

[5] http://seal.web.cern.ch/seal/work-packages/mathlibs/minuit/index.html

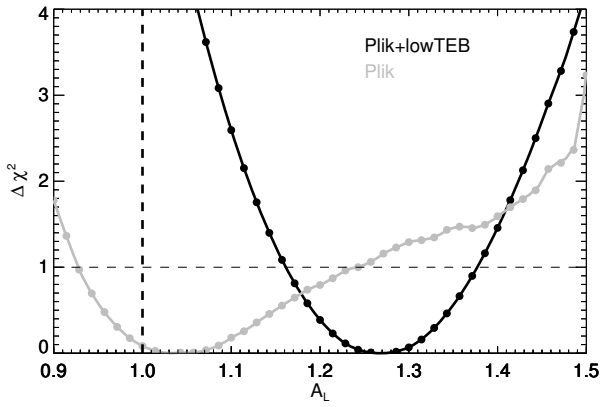

Figure 1. Profile-likelihoods of the A_L parameter reconstructed from the Plik high-ℓ likelihood alone (in grey) and when adding the lowTEB one (in black). The vertical dashed line recalls the expected ΛCDM value.

Figure 1 also shows that the Plik-alone likelihood (in grey) gives:

$$A_L = 1.04^{+0.20}_{-0.10} \quad (\texttt{Plik}, \texttt{class}/\text{profile}), \tag{4}$$

which is compatible with 1.0. This difference from the *Planck* baseline result (Eq. 3) seems to come from a tension between the low and high-ℓ likelihoods. Moreover, using a prior of the kind $\tau = 0.07 \pm 0.02$ (as in Like15) leads to $A_L = 1.16 \pm 0.09$ which goes in the same direction as Plik+lowTEB. This connection with τ will be discussed in the following section.

2.5. High- vs. low-ℓ likelihood results on τ and A_s

We further investigate the high vs. low-ℓ likelihood tensions from the point of view of two other parameters that are strongly correlated to A_L: the reionization optical depth τ and the scalar perturbation amplitude A_s.

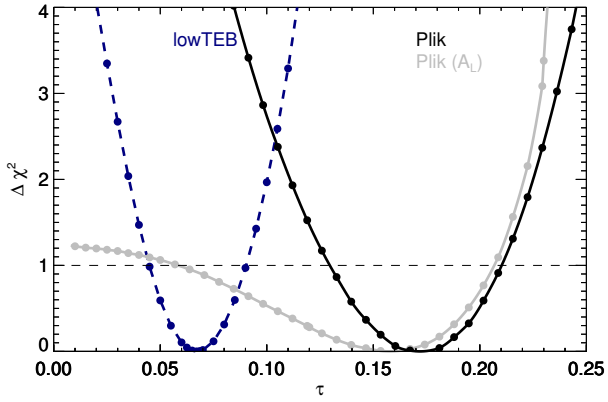

Figure 2. High v.s low-ℓ *Planck* likelihood constraints on τ. The high-ℓ result is obtained with Plik (only) and is shown in black while the low-ℓ one is in dashed blue. Both are obtained within the ΛCDM model. The grey profile shows the result for Plik when A_L is left free in the fits.

Figure 2 shows, in black, the τ profile-likelihood reconstructed with Plik only, which gives:

$$\tau = 0.172^{+0.038}_{-0.042} \quad (\texttt{Plik}). \tag{5}$$

This is higher than the maximum of the posterior reported in Like15 (Fig. 45) that is around 0.14 and is partly due to a volume effect (Sect. 2.3) and partly because of the class/camb difference highlighted in Appendix A. Using consistently class and the same methodology, our result is 2.2σ away from the τ determination with the lowTEB likelihood for which the profile-likelihood gives the same results as the MCMC marginalization (Like15):

$$\tau = 0.067^{+0.023}_{-0.021} \quad (\text{lowTEB}), \tag{6}$$

represented as a blue line on Fig. 2.

Without fixing A_L to 1 (grey curve on Fig. 2) the constraint on τ is much weaker illustrating the fact that the lensing of the CMB anisotropies in the high-ℓ likelihood is the main contributor to the τ measurement. However, some constraining power still remains since the variation of the spectrum with τ is actually more complicated that the simple $\mathcal{A}_T$ scaling (Hu & White 1997).

The discrepancy highlighted in Fig. 2 is directly related to the A_L problem (Fig. 1), but is simpler to study. The high-ℓ likelihood requires a large τ value which is in tension with the low-ℓ-based result. In the A_L test (Fig. 1) one combines both likelihoods. Being the most discriminant, lowTEB pulls τ down. To match the spectra amplitude ($\mathcal{A}_T$), the high-ℓ likelihood pulls A_s down. Then A_L, being fully anti-correlated to A_s (since $C_\ell^\Phi \propto A_L A_s$), shifts to adjust the lensed model to the data again.

Because of the $\mathcal{A}_T$ degeneracy, the Plik-only estimate of A_s is also expected to be high. Indeed from a similar profile-likelihood analysis we obtain:

$$\ln(10^{10} A_s) = 3.270^{+0.058}_{-0.078} \quad (\texttt{Plik}), \tag{7}$$

again discrepant by more than 2σ with the results from Plik+lowTEB, 3.089 ± 0.036 (PCP15).

In summary, the Plik high-ℓ likelihood alone converges to a consistent solution, $A_L \simeq 1$, but with large τ and A_s values. Constraining τ down by adding the lowTEB likelihood (or a low prior) is compensated in the fits by increasing A_L to match the data. To investigate the stability of those results, we will now use another *Planck* high-ℓ likelihoods.

3. The Hillipop likelihood

3.1. Description

Hillipop is one of the *Planck* high-ℓ likelihoods developed for the 2015 data release and is shorty described in Like15. Similarly to Plik, it is a Gaussian likelihood based on cross-spectra from the HFI 100, 143 and 217 GHz maps. The estimate of cross-spectra on data is performed using Xpol, a generalization of the Xspec algorithm (Tristram et al. 2005) to polarization. Figure 3 shows the combined TT spectrum w.r.t the best-fit model that will be deepened later on.

The differences with Plik were mentioned in Like15. The most significant ones are:

- we use all the 15 half-mission cross-spectra built from the 100, 143 and 217 GHz maps while Plik uses only 5 of them;
- we apply inter-calibration coefficients at the map level, resulting in 5 free parameters (one is fixed) while Plik uses 2 at the spectrum level;

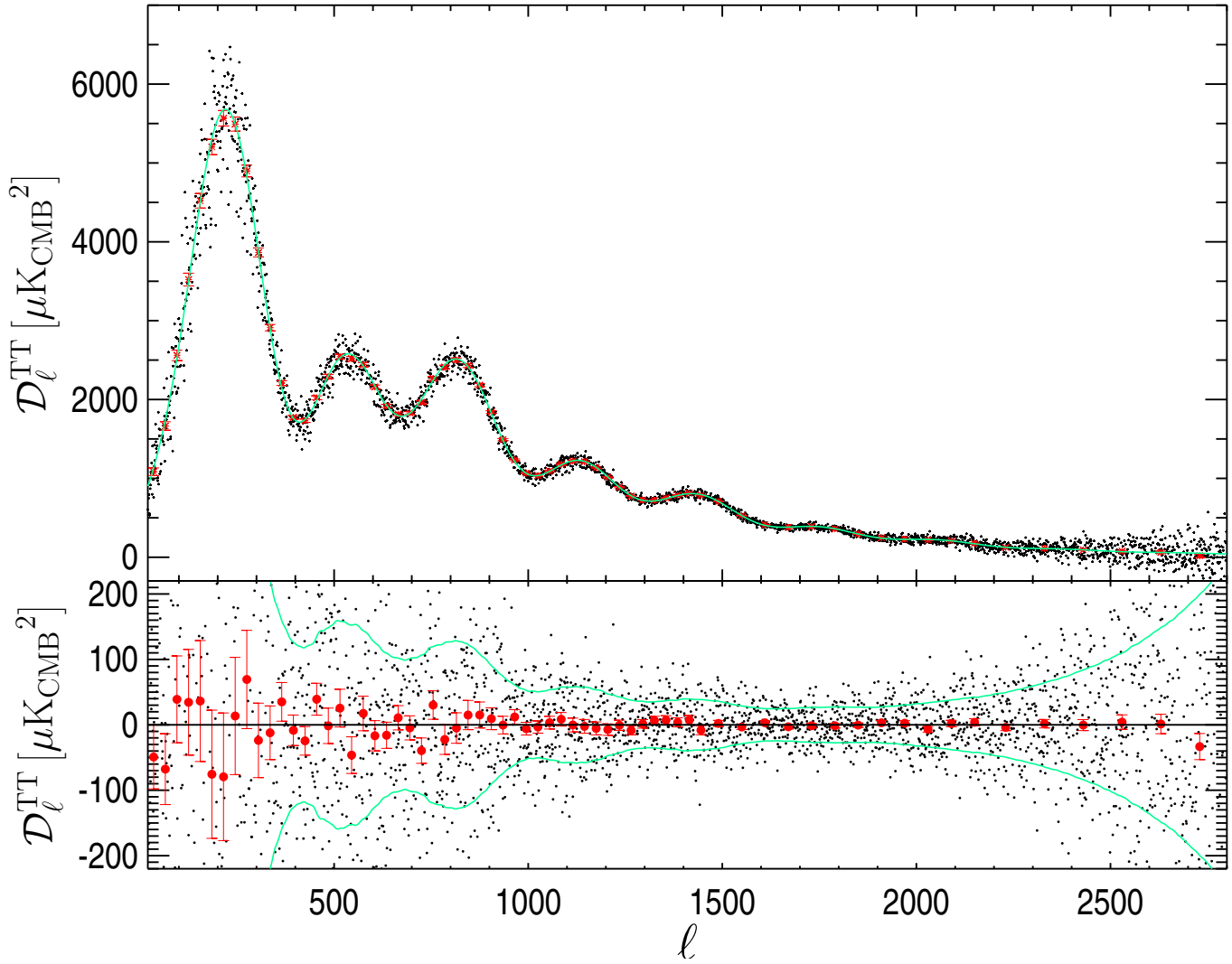

Figure 3. Hillipop foreground-subtracted combined power-spectrum ($\mathcal{D}_\ell = \ell(\ell+1)C_\ell/2\pi$) at each multipole (black points) and binned (red points) w.r.t the best-fit model. The bottom plot shows the residuals. The green line shows the standard deviation as estimated from the covariance matrix.

- we use point-sources masks that were obtained from a refined procedure that extracts Galactic compact structures;
- as a result, our galactic dust component follows closely and is parametrized by the power-law discussed in Planck Collaboration Int. XXX (2014);
- we use foreground templates derived from Planck Collaboration XXX (2014) for the CIB, and Planck Collaboration XXII (2015) for the SZ;
- we use all multipole values (i.e do not bin the spectra).

Using Hillipop leads to ΛCDM estimates very compatible with the other *Planck* ones but on A_s and τ (Like15, Sect. 4.2). Using a prior on τ of 0.07 ± 0.02, we obtain with Hillipop $\tau = 0.075 \pm 0.019$, while `Plik` gives a higher value $\tau = 0.085 \pm 0.018$ (Like15). Given the relation between τ and A_L discussed in Sect. 2.5, we can therefore expect different results on A_L.

3.2. Results

The profile-likelihoods of A_L derived from Hillipop with and without lowTEB is shown in Fig. 4. The Hillipop-alone profile is minimum near $A_L = 1.30$ but is very broad : a 68% CL interval goes from .96 up to 1.42. We therefore conclude that Hillipop alone does not give a strict constraints on A_L. In combination with lowTEB using the same procedure as described in Sect. 2.4 we obtain:

$$A_L = 1.22^{+0.11}_{-0.10} \quad \text{(Hillipop+lowTEB)}. \tag{8}$$

This is slightly lower than the result obtained with `Plik` (Eq. 3) but still discrepant with one by about 2σ.

Within the ΛCDM model, Fig. 5 compares Hillipop vs. lowTEB results on τ. The Hillipop profile on τ gives

$$\tau = 0.134^{+0.038}_{-0.048} \quad \text{(Hillipop)}. \tag{9}$$

This is lower than the `Plik` result with similar error bars (Eq. 5), and lies within 1.3σ of the low-ℓ measurement (Eq. 6). In the

name	definition	prior (if any)
	instrumental	
c_0	map calibration (100-hm1)	1.000 ± 0.002
c_1	map calibration (100-hm2)	1.000 ± 0.002
c_2	map calibration (143-hm1)	fixed to 1.
c_3	map calibration (143-hm2)	1.0000 ± 0.002
c_4	map calibration (217-hm1)	1.0025 ± 0.002
c_5	map calibration (217-hm2)	1.0025 ± 0.002
A	absolute calibration	1.0000 ± 0.0025
	foreground modelling	
$A_{\rm PS}^{100\times100}$	PS amplitude in TT (100x100 GHz)	
$A_{\rm PS}^{100\times143}$	PS amplitude in TT (100x143 GHz)	
$A_{\rm PS}^{100\times217}$	PS amplitude in TT (100x217 GHz)	
$A_{\rm PS}^{143\times143}$	PS amplitude in TT (143x143 GHz)	
$A_{\rm PS}^{143\times217}$	PS amplitude in TT (143x217 GHz)	
$A_{\rm PS}^{217\times217}$	PS amplitude in TT (217x217 GHz)	
$A_{\rm SZ}$	scaling for the tSZ template (TT)	
$A_{\rm CIB}$	scaling for the CIB template (TT)	1.00 ± 0.20
$A_{\rm kSZ}$	scaling for the kSZ template (TT)	
$A_{\rm SZxCIB}$	scaling parameter for the cross correlation between kSZ and CIB	
$A_{\rm dust}^{\rm TT}$	scaling parameter for the dust in TT	1.00 ± 0.20
$A_{\rm dust}^{\rm EE}$	scaling parameter for the dust in EE	1.00 ± 0.20
$A_{\rm dust}^{\rm TE}$	scaling parameter for the dust in TE	1.00 ± 0.20

Table 1. Nuisance parameters for the Hillipop likelihood and Gaussian prior used during the likelihood maximization. The calibration factors are taken from Planck Collaboration VIII (2015) and the amplitude of the dust template extrapolated from the 353 GHz (Planck Collaboration XXX 2014). A prior on $A_{\rm CIB}$ is applied to relieve some degree of degeneracy among foregrounds when ACT+SPT data are not used.

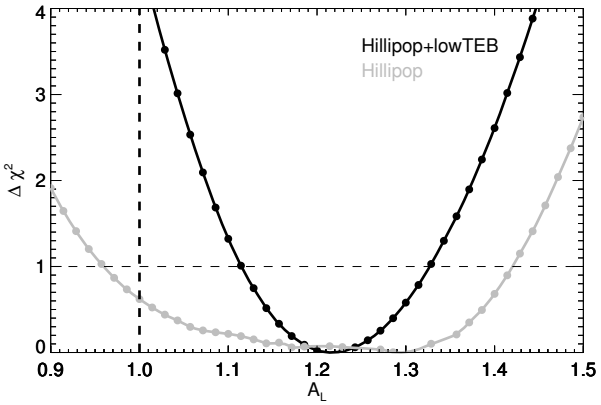

Figure 4. Profile-likelihoods of the $A_{\rm L}$ parameter reconstructed from the Hillipop likelihood alone (in grey) and when adding lowTEB (in black). The vertical dashed line recalls the expected ΛCDM value.

ΛCDM+$A_{\rm L}$ case, Hillipop only gives an upper limit. The difference with `Plik` τ profile (Fig. 2) is the sign of different correlations between $A_{\rm L}$ and τ in these likelihoods.

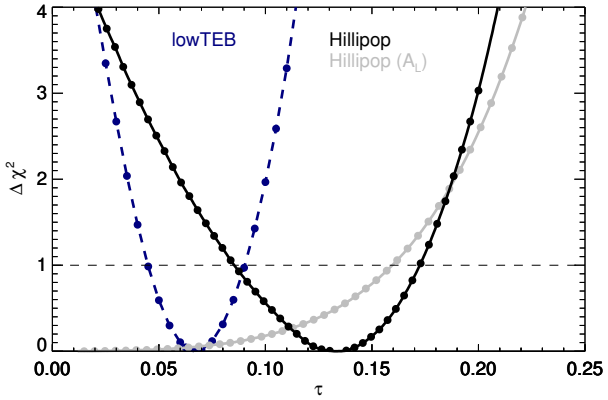

Figure 5. Profile-likelihoods of the τ parameter using only the high-ℓ Hillipop likelihood: ΛCDM+$A_{\rm L}$ free in the fits (in grey) and ΛCDM with fixed $A_{\rm L} = 1$ (in black).

One of the difference between the two likelihoods is in the definition of the foreground models. Moreover, with *Planck* data only, the accuracy on the foreground parameters is weak (especially for SZ and CIB amplitudes). In the next section, we will use the very-high-ℓ datasets. This will both add constraints on lensing through the high multipoles and will better determine the foregrounds parameters and possibly modify the non-trivial correlations between nuisance and cosmological parameters.

4. Adding very-high-ℓ data to constrain the foregrounds

4.1. Datasets

Atacama Cosmology Telescope. We use the final ACT temperature power spectra presented in Das et al. (2014). These are 148×148, 148×218 and 218×218 power spectra built from observations performed on two different sky areas ("south" and "equatorial") and during several seasons, for multipoles between 1000 and 10000 (for 148×148) and 1500 to 10000 otherwise.

South Pole Telescope. We use two distinct datasets from SPT.

The higher ℓ part, dubbed `SPT_high`, uses results, described in Reichardt et al. (2012), from observations at 95, 150 and 220 GHz from the SPT-SZ survey. Their cross-spectra cover the ℓ range between 2000 and 10000. These measurements were calibrated using WMAP 7yr data. A more recent analysis from the complete 24560 deg^2 area of the SPT-SZ survey has been presented in George et al. (2014), dubbed `SPT_high2014` hereafter. In this later release, cross-spectra cover a somewhat broader ℓ range, between 2000 and 13000. Both sets of cross spectra are however quite similar, but the later comes with a covariance matrix that includes calibration uncertainties. Its use makes our work harder as it was calibrated on the *Planck*-2013 data, which in turn had a calibration offset of 1% (at the map level) with respect to the *Planck*-2015 spectra. We thus prefer to use Reichardt et al. (2012) dataset as a baseline in our analyses, with free calibration parameters to match other datasets. We have checked that all results presented in this paper are stable when switching to George et al. (2014), in which case we have to set strict priors on recalibration parameters due to the form of the associated covariance matrix.

We also include the Story et al. (2012) dataset, dubbed SPT_low, consisting of a 150 GHz power spectrum which ranges from $\ell = 650$ to 3000. Some concerns were raised in Planck Collaboration XVI (2014) about the compatibility of this dataset with *Planck* data. The tension was actually traced to be with the WMAP+SPT cosmology and the *Planck* and SPT_low power spectra were found to be broadly consistent with each other (Planck Collaboration XVI 2014). As will be shown later, we do not see any sign of tension between the *Planck*-2015 data and the SPT_low dataset nor some reason to exclude it.

4.2. Foregrounds modelling

For the very-high-ℓ astrophysical foregrounds, we chose to use a model as coherent as possible with what has been set-up for Hillipop, i.e. the same templates for tSZ, kSZ, CIB and kSZ×CIB. Since they have been computed for the *Planck* frequencies, we have to extrapolate them to the ACT and SPT frequencies and bandpasses. For tSZ, we scale the template with the usual $f_\nu = x \coth x/2 - 4$ function (where $x = h\nu/k_B T_{CMB}$), using the effective frequencies given in Dunkley et al. (2013). For CIB and tSZ×CIB, we start from templates in $Jy^2.sr^{-1}$ in the IRAS convention ($\nu I(\nu)$ = cste spectrum) for *Planck* frequencies and bandpasses. For CIB, we use the conversion factors from *Planck* to the ACT/SPT bandpasses, assuming the Béthermin et al. (2012) SED for the CIB combined with unit conversion factors to K_{CMB}, for the ACT and SPT bandpasses (Lagache 2014). These factors are given in Table 2.

Dataset	Frequency (GHz)	$MJy.sr^{-1}/K_{CMB}$	HFI freq. (GHz)	conversion
ACT	148	401.936	143	0.85
	218	485.311	217	1.056
SPT	95	234.042	100	1.090
	150	413.540	143	0.7688
	220	477.017	217	1.061

Table 2. Conversion factors used for the foreground template extrapolation to ACT and SPT bandpasses with the CIB SED.

For the tSZ×CIB component of the $(\nu_1 \times \nu_2)$ cross-spectrum (from the ACT or SPT dataset), we scale the nearest HFI cross-spectrum $(\nu_1^P \times \nu_2^P)$ using the ratio :

$$S_{\nu_1,\nu_2} = \frac{f_{\nu_1} C_{\nu_2} + f_{\nu_2} C_{\nu_1}}{f_{\nu_1^P} C_{\nu_2^P} + f_{\nu_2^P} C_{\nu_1^P}} \quad (10)$$

and then convert it to K_{CMB} using the above factors. This scaling applies at the 15% level for the HFI cross-frequency templates, choosing the 143×143 one as a reference.

On top of this, a few more specific templates have been added to each datasets :

- Point sources : to mask resolved point sources, ACT and SPT used their own settings to match each instrument's sensitivity and angular resolution. The unresolved point source populations in each case are thus different, so we introduce extra nuisance parameters to model them. We model the unresolved point source components in the ACT and SPT spectra with one amplitude $A_{PS}^{\nu_1\times\nu_2}$ parameter per cross-spectrum. This hence introduces six nuisance parameters for the ACT, six for the SPT_high and one for the SPT_low datasets, respectively (cf. Table 3).
- Galactic dust : following Dunkley et al. (2013) and Das et al. (2014), we model the dust contribution in the ACT power spectra as a power law :

$$\mathcal{D}_\ell^{dust}(i,j) = A_{\rm dust}^{\rm ACT} \left(\frac{\ell}{3000}\right)^{-0.7} \left(\frac{\nu_i \nu_j}{\nu_0^2}\right)^{3.8} \left[\frac{g(\nu_i) g(\nu_j)}{g(\nu_0)^2}\right] \quad (11)$$

We therefore introduce two nuisance parameters, one for each part of the ACT dataset, and set the reference frequency ν_0 at 150 GHz.
For the SPT datasets, following Reichardt et al. (2012), we use a fixed template, with amplitudes 0.16, 0.21 and 2.19 μK^2_{CMB} at 95, 150 and 218 GHz, respectively and an $\ell^{-1.2}$ spatial dependency.

4.3. Likelihoods

We compute one likelihood for each of the five very-high-ℓ datasets following the method described in Dunkley et al. (2013). We use the respective published window functions to bin the (CMB + foregrounds) model, and the released covariance matrices to compute the likelihood. In all cases, these include beam uncertainties.

Since we combine different datasets, we introduced 9 additional nuisance parameters to account for their relative calibration uncertainties (at map level).

Figure 6 shows a comparison of all the foreground-subtracted CMB spectra for the 150×150 component (which is almost common to all experiments), and Table 3 summarizes the characteristics of the datasets we use in the VHL likelihoods.

A detailed inspection of all cross-spectra per frequency and component has been performed and does not reveal any inconsistency with the *Planck* data. More details are given in Appendix C.

Dataset	freq (GHz)	#spectra	#nuisances
SPT_low	150	1	2
SPT_high	95, 150, 220	6	9
ACT south/equat . . .	148, 218	6	12

Table 3. Summmary of the characteristics of the very-high-ℓ data used in this analysis. Each experiment's likelihood includes map calibrations and residual point source levels, which results in a number of additional nuisance parameters showed in the last column. In combined fits, the SZ and CIB foreground templates are common with Hillipop.

4.4. First results and global consistency check

We first check that the combination of the ACT+SPT likelihoods (hereafter VHL) gives results consistent with Hillipop. For this purpose we sample independently the Hillipop and VHL likelihoods and compare their ΛCDM estimates in Fig. 7. Both datasets lead to similar cosmological parameters. However, an accurate measurement of $\Omega_b h^2$ and $\Omega_c h^2$ requires a precise determination of the relative amplitudes of the CMB acoustic peaks for which

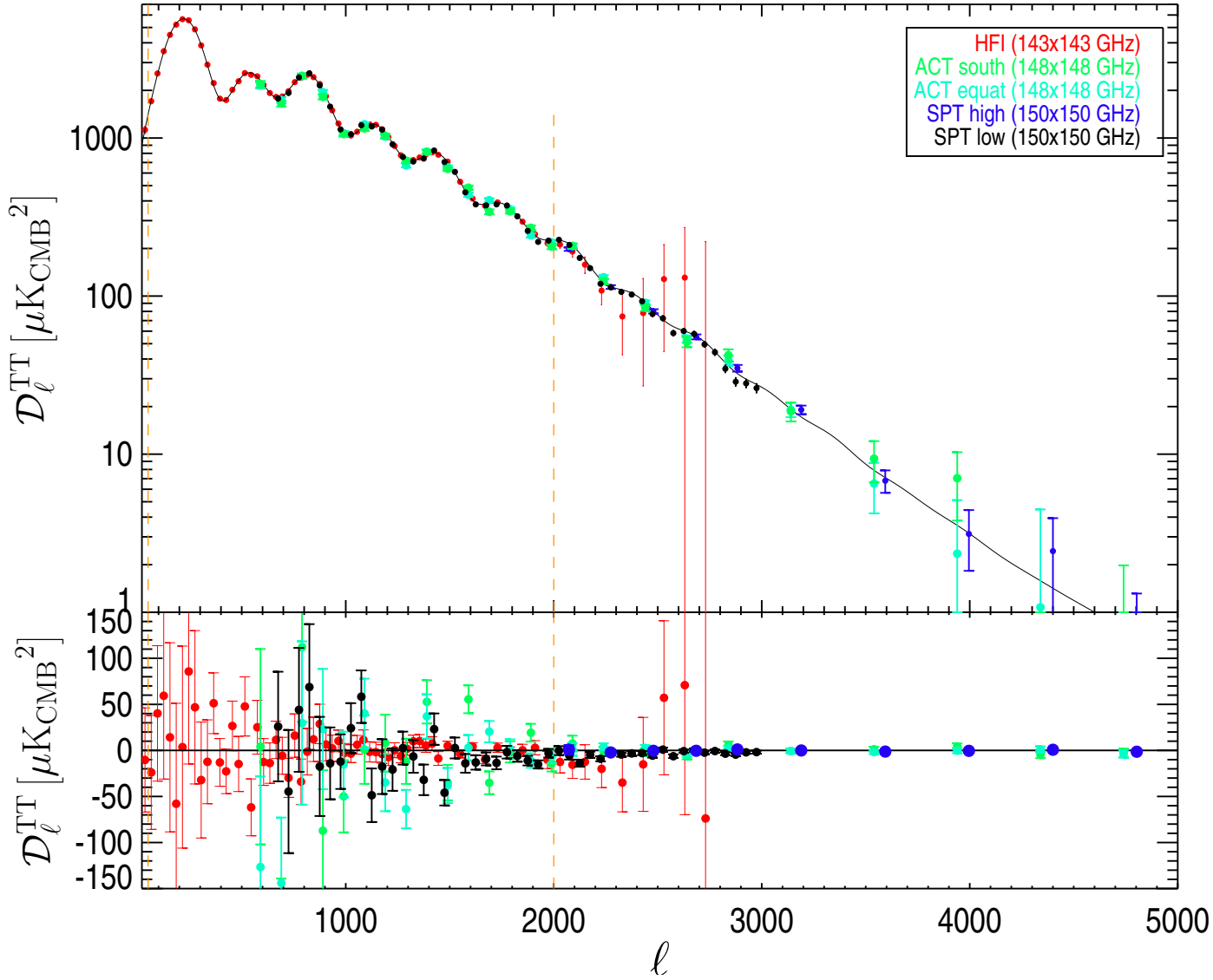

Figure 6. Foreground-subtracted CMB cross-spectra of all the experiments used at ≃ 150 GHz. The full line is the best fit of the Hillipop+VHL combination and is subtracted to obtain the bottom residual plot. The Hillipop likelihood uses individual multipoles up to 2000 and window functions have been accounted for in the very-high-ℓ data.

the very-high-ℓ datasets are less sensitive. This is reflected by the width of the posteriors shown in Fig. 7.

The χ^2 contributions to the Hillipop+VHL+lowTEB best fit of each of the very-high-ℓ datasets are 58 /47(d.o.f.), 77 /90 and 651/710 for the `SPT_low`, `SPT_high` and `ACT` datasets, respectively. None of these individual values indicate strong tension between the likelihood parts. Note that in all cases, the covariance matrices provided by the ACT and SPT groups, and used to compute the χ^2, include non negligible non-diagonal elements. For example, the visual impression from the `SPT+low` residuals, shown on Fig. C.3 is not excellent, but the χ^2 from this part of the fit given above has a PTE of 13% which is perfectly acceptable.

4.5. A_L and τ results

In a second step, we perform the same analysis as in Sects. 2 and 3.2 adding the VHL likelihood to Hillipop and consider the A_L profile-likelihood (with lowTEB) in Fig. 8. The result becomes:

$$A_L = 1.03 \pm 0.08 \quad \text{(Hillipop+lowTEB+VHL)}, \qquad (12)$$

now fully compatible with one.

As we will see in Sect. 5, the inclusion of the VHL data does not change much the cosmological parameters but, as expected, strongly constrains all the foregrounds including, through correlations, the ones specific to *Planck* data (dust and point source amplitudes). This is shown in Fig. 9.

It is worth recalling that all Hillipop nuisance amplitudes (but the point sources) represent coefficients scaling foreground templates: it is remarkable that after adding the VHL likelihood they all lie reasonably (at least those for which we have the sensitivity) around one, which is a strong support in favor of the coherence of the foregrounds description.

For τ, combining the VHL with the Hillipop likelihood removes any sign of tension with lowTEB as shown in Fig. 10, and we obtain:

$$\tau = 0.052 \pm 0.035 \quad \text{(Hillipop+VHL)}, \qquad (13)$$

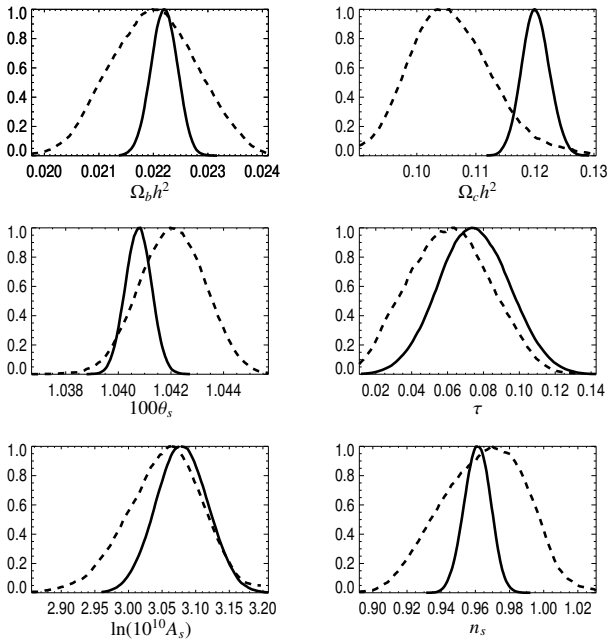

Figure 7. Posterior distributions of the cosmological parameters obtained by sampling the Hillipop (full line) and ACT+SPT (dashed) likelihoods independently. A prior of $\tau = 0.07 \pm 0.02$ is used in both cases. For clarity we only show the cosmological parameters but all nuisances are sampled.

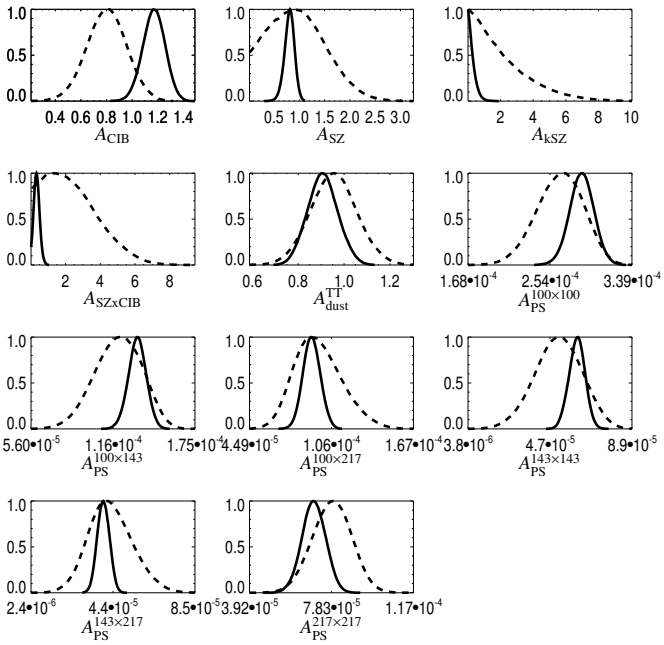

Figure 9. Posterior distributions of the foreground Hillipop parameters with (full line) and without (dashed line) the VHL likelihood The definition of each parameter can be found in Table 1.

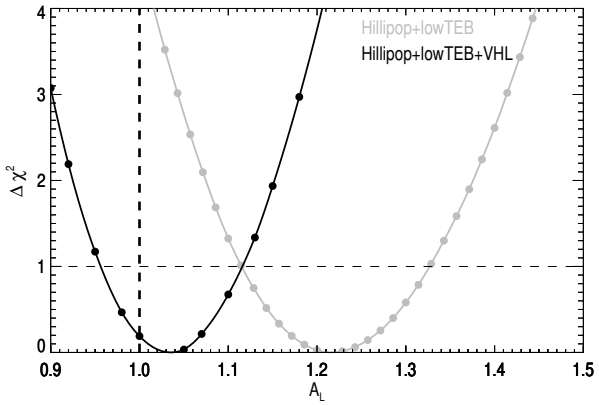

Figure 8. Profile-likelihood for $A_{\rm L}$ reconstructed from the Hillipop+lowTEB likelihood (in grey) and adding the very-high-ℓ ACT and SPT data ('VHL') discussed in the text (in black).

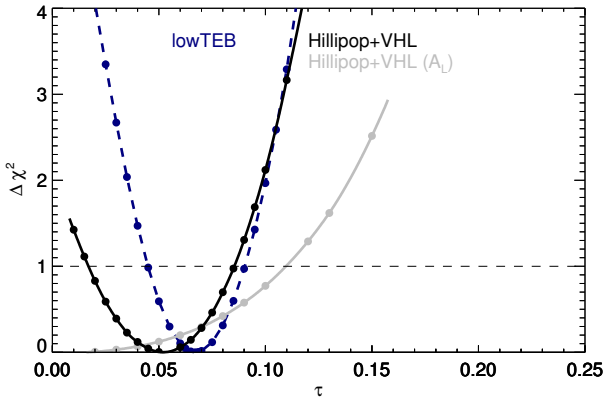

Figure 10. Hillipop+VHL and lowTEB likelihood constraints on τ. The grey profile shows the result for Hillipop+VHL when $A_{\rm L}$ is left free in the fits. The lowTEB one is in dashed blue.

in excellent agreement with the lowTEB measurement (Eq. 6).

4.6. Systematic checks

Effect of correlations. In order to study whether the improvement observed when adding the VHL data comes only from a more precise determination of the various foreground levels, we perform the following measurement: we use the Hillipop+lowTEB likelihood to determine $A_{\rm L}$ as in Sect. 3.2 but fixing all the nuisance parameters to the best-fit value of Hillipop+lowTEB+VHL. The $\chi^2_{\rm min}$ value increases from 20443 with all free parameters to 20456 when fixing the nuisances which is significantly higher. $A_{\rm L}$ in the latter case is 1.10 ± 0.08 which is only half-way from the full VHL results (Eq. 12) and with similar errors. These results suggest that the information brought by the VHL data on the nuisance parameters is not only due to a more precise determination of their mean levels and that correlations play a sizable role in particular on the $A_{\rm L}$ central value.

SZ correlations. As discussed in Sect. 2.1, *Planck* included the very-high-ℓ information in the `Plik` likelihood through a linear constraint between the thermal and kinetic components of the SZ foreground. When combining Hillipop with the VHL likelihood, a similar correlation is observed which reads in our conventions:

$$A^{\rm kSZ} + 3.5A^{\rm tSZ} = 3.16 \pm 0.25 \qquad (14)$$

To check whether this correlation is sufficient to capture the essentials of the very-high-ℓ information, we re-run the profile analysis adding to Hillipop+lowTEB only the prior in Eq. 14 and

measure:

$$A_L = 1.26^{+0.12}_{-0.10} \quad \text{(Hillipop+lowTEB+SZ-cor)}. \qquad (15)$$

Comparison with Eq. 8 shows that using this correlation does not capture in our case the complexity of the full covariance matrix.

Robustness of the results. We tested a large number of configurations of the VHL dataset to establish whether the improvement comes from a peculiar one. Results are presented in Table. 4.

Dataset	A_L
`None`	1.22 ± 0.11
`SPT_low`	1.16 ± 0.10
`SPT_high`	1.12 ± 0.10
`ACT`	1.19 ± 0.10
`SPT_low` + `SPT_high`	1.02 ± 0.08
`SPT_low` + `ACT`	1.09 ± 0.09
`SPT_high` + `ACT`	1.12 ± 0.09
`SPT_low` + `SPT_high` + `ACT`	1.04 ± 0.08
`SPT_low` + `SPT_high2014` + `ACT`	1.03 ± 0.08

Table 4. Results on A_L using Hillipop+lowTEB and various dataset combinations on the VHL side. For their exact definition see Sect. 4.

It is difficult to draw firm conclusions from this exercise, since the number of extra nuisances parameters is varying in each case (see Table. 3). The improvement on A_L is most significant when combining several datasets but also satisfactory as soon as one combines at least two of them. Note that all those results are highly correlated with each other, as they all make use of Hillipop. Even though one may prefer central values very close to 1.0, it must be pointed out that there are several combinations compatible with 1.0 at the $\sim 1\sigma$ level. This may indicate that the better the constraint on the high end of the power spectrum, the better the constraint on the A_L control parameter (the lensing effect on C_ℓ^{TT} is not only a smearing of peaks and troughs but also a redistribution of power towards the high ℓ, above ~ 3000).

Since we have seen that the A_L improvement partly comes from the correlations, it is reasonable to assume that the foregrounds covariance is better constrained by several measurements.

Finally, we noticed that the `SPT_high` 220×220 spectrum lies slightly high with respect to the best-fit (see Appendix C). Indeed we get a better agreement in this case by increasing the contribution of the SPT dust amplitude. To check the impact on A_L, we re-run the analysis multiplying the dust level for all SPT spectra, $A^{\rm SPT}_{\rm dust}$, by a factor 3 and obtain:

$A_L = 1.13 \pm 0.10$ (Hillipop+lowTEB+SPT_high, $A^{\rm SPT}_{\rm dust}\times 3$)

$A_L = 1.04 \pm 0.08$ (Hillipop+lowTEB+VHL, $A^{\rm SPT}_{\rm dust}\times 3$).

Comparison with Table 4 shows that the details of the SPT dust amplitude do not affect the final results.

5. Results on ΛCDM parameters

We have shown how the Hillipop likelihood is regularized by including the very-high-ℓ data. We have checked that it leads to results fully compatible with the lowTEB likelihood for τ and that their combination leads to an A_L value now compatible with one. We then combine the three likelihoods and fix A_L to one, to evaluate the impact on ΛCDM parameters. The comparison with the *Planck* published result is shown in Fig. 11. We note that:

- `Plik` and Hillipop likelihoods share essentially the same data;
- the problem pointed out by A_L is not a second-order effect: it directly affects Ω_b, τ, and A_s results;
- our regularized likelihood provides a lower σ_8 estimate.

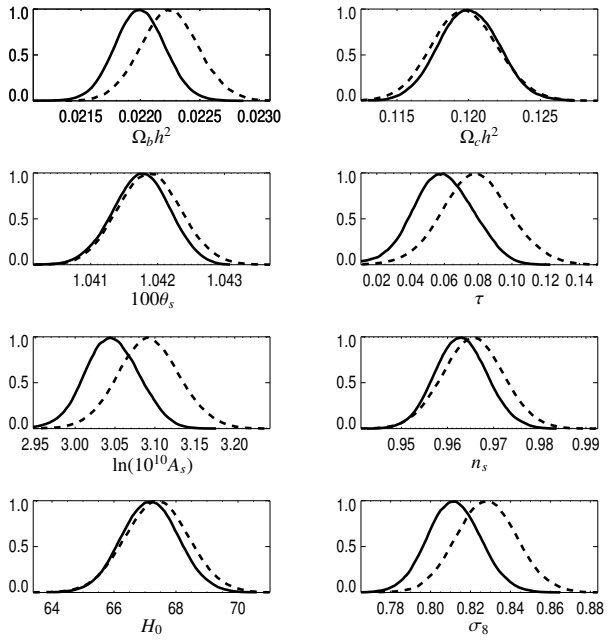

Figure 11. Posterior distributions of the ΛCDM cosmological parameters obtained with our regularized likelihood (Hillipop+lowTEB+VHL, full line), compared to the *Planck* baseline result (`Plik`+lowTEB, dashed line). We recall this latter also includes some VHL information through an SZ correlation discussed in PCP15. The last row shows derived parameters.

These results are obtained using only CMB data. To check the overall consistency and constrain the parameters we also make use of some robust extra-information by including recent BAO and supernovae results.

The Baryon Acoustic Oscillations (BAO) are generated by acoustic waves in the primordial fluid, and can be measured today through the study of the correlation functions of galaxy surveys. Due to the fact that their measurement is sensitive to different systematic errors than the CMB, they help breaking the degeneracies, and are therefore further used in this paper to constrain the cosmological parameters. We have used here: the acoustic-scale distance ratio $D_V(z)/r_{drag}$ measurements[6] from the 6dF Galaxy Survey at $z = 0.1$ (Beutler et al. 2014), and from BOSS-LowZ at $z = 0.32$. They have been combined with the BOSS-CMASS anisotropic measurements at $z = 0.57$. considering both the line-of-sight and the transverse direction as described in Anderson et al. (2014).

Type Ia supernovae (SN) had a major role in the discovery of late time acceleration of the Universe and constitutes a powerful

[6] $D_V(z)$ is a function of the redshift (z) and can be expressed in terms of the angular diameter distance and the Hubble parameter, r_{drag} is the comoving sound horizon at the end of the baryon drag epoch.

cosmological probe complementary to CMB constraints. We have used the JLA compilation (Betoule et al. 2014) which covers a wide redshift range (from 0.01 to 1.2).

Table 5 gives the results obtained with Hillipop+lowTEB (ie. using only *Planck* data), then adding ACT+SPT likelihoods (ie. only CMB) and finally adding also the BAO and SNIa likelihoods.

Using only *Planck* data, the Hillipop+lowTEB results (first column in Table 5) are almost identical to the ones reported for '*Planck* TT+lowP' in PCP15, but for τ and A_s that are smaller, as explained in Sects. 3.2 and 2.5.

As discussed throughout this paper, adding the very-high-ℓ data (second column) releases the tension on the optical depth, leading to a value of τ around 0.06, as can be anticipated from Fig. 10. We also see a slight shift of $\Omega_b h^2$ that is difficult to analyze since at this level of precision, this parameter enters several areas of the Boltzmann computations (e.g., Hu & White 1997).

Then, adding the BAO and SN data (third column) increases the precision on the parameters but does not change substantially their value.

Note that in all cases, σ_8 is stable, e.g. Hillipop+lowTEB gives $\sigma_8 = 0.816 \pm 0.015$. This is only in mild tension with other astrophysical determinations such as weak lensing (Heymans et al. 2013) and Sunyaev-Zeldovich cluster number counts (Planck Collaboration XXIV 2015).

6. Conclusion

In this work we investigated the deviation of the A_L parameter from unity and found it to be of 2.6σ, using the `Plik` high-ℓ and lowTEB low-ℓ *Planck* likelihoods. For these demanding tests, we chose to consistently use the profile-likelihood method, which is well suited to such studies. We first showed how this A_L deviation is related to a difference in the τ estimations when performed using `Plik` or lowTEB alone.

The Hillipop likelihood has been built based on different foreground and nuisance parametrization. We showed that Hillipop alone is only very loosely constraining A_L towards high values, and that its τ estimate lies closer to the low-ℓ measurement, albeit on the high-end side.

We then added to Hillipop, high angular resolution CMB data from the ground-based ACT and SPT experiments to further constrain the high-ℓ part of the CMB power spectrum and the foreground parameters. Cosmological parameters derived from this setup are shown to be more self-consistent, in particular the reconstructed τ value is coherent with the low-ℓ determination extracted from the lowTEB likelihood. They also pass the $A_L = 1$ test.

We showed that this regularization is quite robust against the details of the very-high-ℓ datasets used, and specific foreground hypotheses. We also showed that it is not only related to a better determination of the foreground amplitudes but also seems to lie in their correlations.

The cosmological parameters determined from this combined CMB likelihood are also stable when adding BAO and SNIa likelihoods. This is in particular the case for σ_8 that we always find close to 0.81. With respect to the cosmological parameters derived by the *Planck* collaboration, the main differences concern τ, and A_s to which the former is directly correlated, and $\Omega_b h^2$, which shifts by a fraction of σ. Other parameters are almost identical.

Improving on A_L is a delicate task and it seems that the source of the regularization cannot be easily pinpointed. The choices of the Hillipop likelihood impact on the correlations between all the parameters, yielding a τ estimate in smaller tension with the low-ℓ likelihood. But this was not sufficient to relieve the A_L tension. It is only by further constraining foregrounds using very-high-ℓ likelihoods that we were able to obtain a coherent picture over a broad multipole range. The source of the tiny improvement probably lies in the details of the full parameters covariance matrix.

One cannot exclude that the A_L deviation from unity still partly results from an incomplete accounting of some residual systematics in the ACT, SPT or *Planck* data. It will thus be worthwhile to reexamine this question with their future releases.

Acknowledgements. We thank Guilaine Lagache for building and providing the point-source masks cleaned from Galactic compact structures, Marian Douspis for providing the SZ templates, and Marc Betoule for the development of the `C` version of the `JLA` likelihood.

Appendix A: `class` vs. `camb` results

Our results were obtained using the `class v2.4.3` Boltzmann code, which computes the temperature and polarization power spectra by evolving the cosmological background and perturbation equations. Besides being very clearly written in `C` and modular, `class` has a very complete set of *precision parameters* in a single place that allows to study them efficiently. This makes it a perfect tool for developing modern high-precision cosmological projects.

We revisit the agreement between `class` and `camb` at the level required to estimate A_L. For this purpose, we fix the cosmology to the *Planck* TT+lowP best-fit and run `class` with 3 different settings:

- the *default* ones for v2.4.3;
- the *high-quality* (HQ) ones that are being used to obtain some smooth profile-likelihoods and are given in Table B.1;
- the *very high-quality* (VHQ) ones corresponding to the maximal precision one can reasonably reach on a cluster[7] and that are provided in `class` in the file `cl_ref.pre`.

For `camb` we use the corresponding spectrum released in the *Planck* Legacy Archive. We compare the spectra on Fig. A.1

Generally speaking the agreement is at the $(\mu K)^2$ level which is below one percent agreement over the whole range. In practice this means it does not impact the ΛCDM parameters as discussed in Like15.

The low-ℓ difference is not very important for data analysis since experiments are limited there by the cosmic variance. The asymptotic $\simeq 1(\mu K)^2$ offset is more worrying and some ΛCDM extensions could be sensitive to this difference. Since the `class` spectrum is slightly lower than the `camb` one precisely in the high-ℓ region where A_L has the largest impact, it should lead to a higher A_L value. This is indeed observed and discussed in Sect. 2.4 but has a small effect on A_L.

Finally we note that all `class` settings give similar results, in particular in their high-ℓ region, and that our HQ settings (used for profile-likelihoods) are smoother than the default ones and similar to the most extreme ones (VHQ).

Appendix B: Optimization of profile-likelihoods

The computation of genuine profile-likelihoods requires exquisite minimization precision. Since the 68% confidence intervals are

[7] This single shot run last several minutes on 8 cores and requires about 30GB of memory

Parameter	Hillipop+lowTEB	Hillipop+lowTEB +VHL	Hillipop+lowTEB +VHL+BAO+SN
$\Omega_b h^2$	0.02221 ± 0.00023	0.02200 ± 0.00019	0.02207 ± 0.00018
$\Omega_c h^2$	0.1192 ± 0.0022	0.1200 ± 0.0020	0.1187 ± 0.0012
$100\theta_s$	1.04175 ± 0.00044	1.04200 ± 0.00040	1.04188 ± 0.00036
τ	0.072 ± 0.020	0.059 ± 0.017	0.063 ± 0.017
n_s	0.9645 ± 0.0071	0.9630 ± 0.0054	0.9663 ± 0.0040
$\ln(10^{10}A_s)$	3.068 ± 0.038	3.045 ± 0.032	3.050 ± 0.032
Ω_m	0.311 ± 0.013	0.315 ± 0.012	0.308 ± 0.007
H_0	67.51 ± 0.97	67.19 ± 0.88	67.72 ± 0.53
σ_8	0.816 ± 0.015	0.811 ± 0.013	0.810 ± 0.013

Table 5. Estimates of cosmological parameters using MCMC techniques for the six ΛCDM parameters. First with our likelihood (Hillipop) and lowTEB. Then with our regularized likelihood (Hillipop+lowTEB+VHL, second column) and further adding some BAO and SN data (third column). Here θ_s, as computed by `class`, represents the exact angular size of the sound horizon and should not be identified to the `CosmoMC` θ_{MC} parameter (see Appendix B).

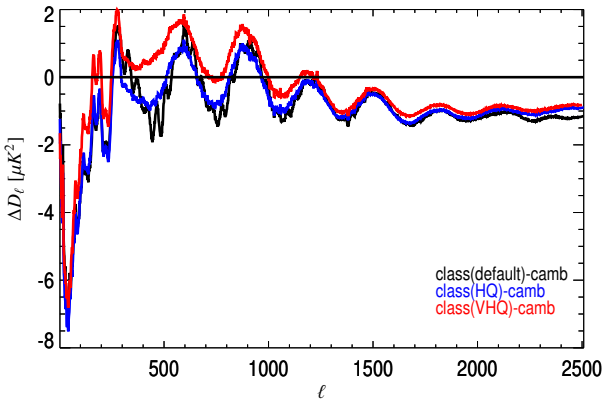

Figure A.1. Difference of $D_\ell \equiv \ell(\ell+1)C_\ell^{TT}/2\pi$ power spectra between `class` and `camb` for the same fiducial cosmology. For `class` several precision settings are tested: the default ones (in black), the high-quality (in blue) and very high-quality ones (in red) as described in the text.

`class` parameter	Value
tol_background_integration	10^{-3}
tol_thermo_integration	10^{-3}
tol_perturb_integration	10^{-6}
reionization_optical_depth_tol	10^{-5}
l_logstep	1.08
l_linstep	25
perturb_sampling_stepsize	0.04
delta_l_max	1000
accurate_lensing	1

Table B.1. High-precision settings of the `class` non-default parameters used in the profile-likelihood constructions. The last parameter (accurate_lensing) is only useful (and used) to model in details the very-high-ℓ tail (typically above 4000) and is only used with our ACT and SPT likelihoods.

obtained by thresholding the profiles at 1, we need a precision on $\chi^2_{\rm min}$ well below 0.1 which is challenging for a numerical method without analytic gradients. It was already shown in Planck Collaboration Int. XVI (2014) how using the `Minuit` package and increasing the `class` precision parameters to high values (still keeping a reasonable computation time) allows to achieve this goal.

Besides revisiting our high-precision parameters that are shown in Table B.1, we have further improved our strategy using the following scheme:

1. we use the `pico` software[8] to pre-compute a best fit solution. `pico` is based on the interpolation between spectra trained on the `camb` Boltzmann solver, it is very fast and the minimization converges rapidly due to the smoothness between models.
2. since `camb` computes only an approximation of the angular size of the sound horizon (θ_{MC}) while `class` computes it exactly (θ_s) we perform the change of variables by fixing the previous best-fit estimates and performing a 1D fit to θ_s only.
3. we then have a good starting point to `class` and perform the minimization with a high precision strategy (`Migrad`, strategy=2 level).
4. optionally: in some rare cases, the estimated minimum is not accurate enough (this can be identified by checking the profile-likelihood continuity). In this case, we use several random initialization points (typically 10) near the previous minimum, perform the same minimization, and keep the lowest χ^2_{min} solution.

In all cases we have checked that the `pico` results are similar to the final `class` ones but consider the latter to give more precise results since `pico` implements only an approximation to the A_L parameter and was trained on an old `camb` version.

[8] https://sites.google.com/a/ucdavis.edu/pico

Appendix C: very-high-ℓ consistency

We give here more details on the checks we performed in order to assess the ACT, SPT and *Planck* spectra compatibility in the very-high-ℓ regime. Fig. C.1, C.2 and C.3 show the detailed fit of each component for each dataset. The components are obtained from the templates scaled according to the combined Hillipop+lowTEB+VHL fitted cosmological and nuisance parameters. The general agreement on the very-high-ℓ side is very good as shown by the χ^2 for each dataset given in Sect. 4.4. Note that the points are largely correlated and that the exact χ^2 computation involves the full covariance matrices provided by each experiment, which all contain non negligible off-diagonal terms. For example, the χ^2 from the `SPT_low` part is 58 for 47 degrees of freedom which has a 13% PTE. Some small excess in data seems to show up in the `SPT_high` 220×220 GHz spectrum above $\ell = 3000$. It is checked in Sect. 4.6 that this does not influence any of our results.

References

Anderson, L., Aubourg, É., Bailey, S., et al. 2014, MNRAS, 441, 24, arXiv:1312.4877
Béthermin, M., Daddi, E., Magdis, G., et al. 2012, ApJ, 757, L23, arXiv:1208.6512
Betoule, M., Kessler, R., Guy, J., et al. 2014, arXiv, 4064, arXiv:1401.4064
Beutler, F. et al. 2014, Mon.Not.Roy.Astron.Soc., 444, 3501, arXiv:1403.4599
Blanchard, A. & Schneider, J. 1987, A&A, 184, 1
Calabrese, E., Slosar, A., Melchiorri, A., Smoot, G. F., & Zahn, O. 2008, Phys. Rev. D, 77, 123531, arXiv:0803.2309
Das, S., Louis, T., Nolta, M. R., et al. 2014, J. Cosmology Astropart. Phys., 4, 14, arXiv:1301.1037
Di Valentino, E., Melchiorri, A., & Silk, J. 2015, ArXiv e-prints, arXiv:1509.07501
Dunkley, J., Calabrese, E., Sievers, J., et al. 2013, J. Cosmology Astropart. Phys., 7, 25, arXiv:1301.0776
George, E. M., Reichardt, C. L., Aird, K. A., et al. 2014, ArXiv e-prints, arXiv:1408.3161
Heymans, C. et al. 2013, Mon. Not. Roy. Astron. Soc., 432, 2433, arXiv:1303.1808
Hu, B. & Raveri, M. 2015, Phys. Rev. D, 91, 123515, arXiv:1502.06599
Hu, W. & White, M. 1997, ApJ, 479, 568, arXiv:astro-ph/9609079
James, F. 2007, Statistical Methods in Experimental Physics (World Scientific)
Lagache, G. 2014, Planck internal note
Lesgourgues, J. 2011a, ArXiv e-prints, arXiv:1104.2932
Lesgourgues, J. 2011b, ArXiv e-prints, arXiv:1104.2934
Lewis, A. & Challinor, A. 2006, Phys. Rep., 429, 1, arXiv:astro-ph/0601594
Lewis, A., Challinor, A., & Lasenby, A. 2000, ApJ, 538, 473, arXiv:astro-ph/9911177
Planck Collaboration XVI. 2014, A&A, 571, A16, arXiv:1303.5076
Planck Collaboration XXX. 2014, A&A, 571, A30, arXiv:1309.0382
Planck Collaboration I. 2015, in preparation
Planck Collaboration VIII. 2015, in preparation
Planck Collaboration XI. 2015, ArXiv e-prints, arXiv:1507.02704
Planck Collaboration XIII. 2015, ArXiv e-prints, arXiv:1502.01589
Planck Collaboration XXII. 2015, in preparation
Planck Collaboration XXIV. 2015, in preparation
Planck Collaboration Int. XVI. 2014, A&A, 566, A54, arXiv:1311.1657
Planck Collaboration Int. XXX. 2014, A&A, in press, arXiv:1409.5738
Porter, F. 1996, Nuclear Instruments and Methods in Physics Research A, 368, 793
Reichardt, C. L., Shaw, L., Zahn, O., et al. 2012, ApJ, 755, 70, arXiv:1111.0932
Story, K. T., Reichardt, C. L., Hou, Z., et al. 2012, ArXiv e-prints, arXiv:1210.7231
Tristram, M., Macías-Pérez, J. F., Renault, C., & Santos, D. 2005, MNRAS, 358, 833, arXiv:astro-ph/0405575

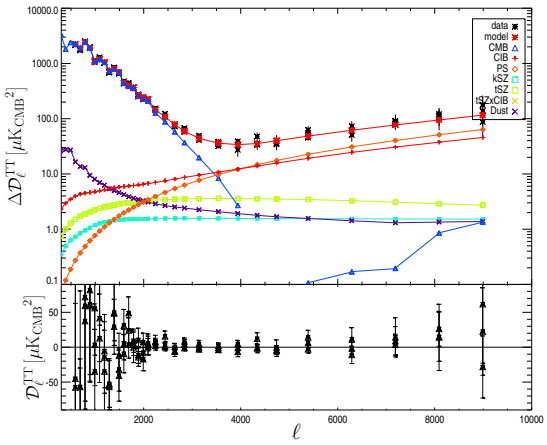

(a) ACT_equat 148×148 GHz

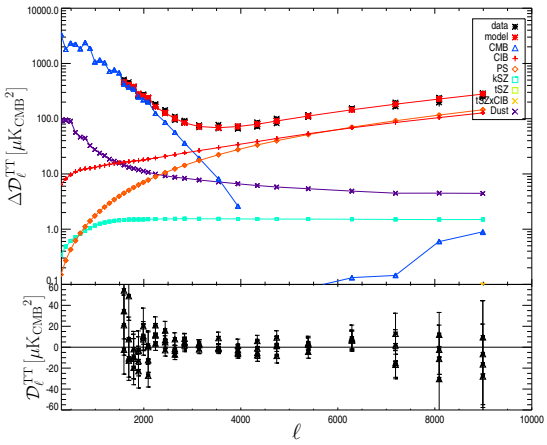

(b) ACT_equat 148×218 GHz

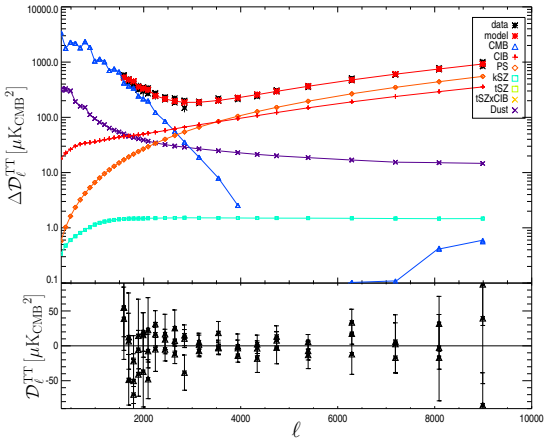

(c) ACT_equat 218×218 GHz

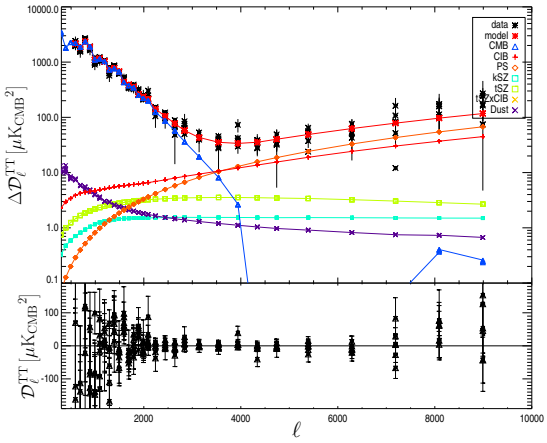

(d) ACT_south 148×148 GHz

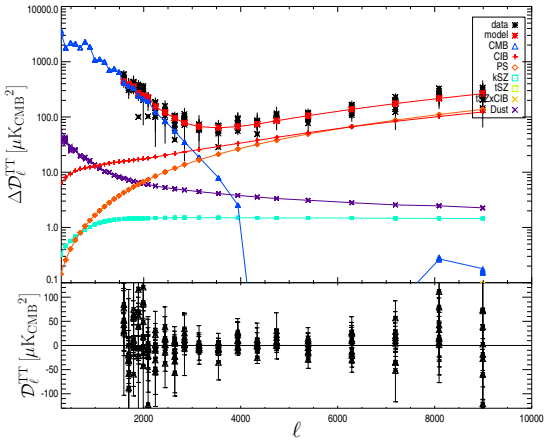

(e) ACT_south 148×218 GHz

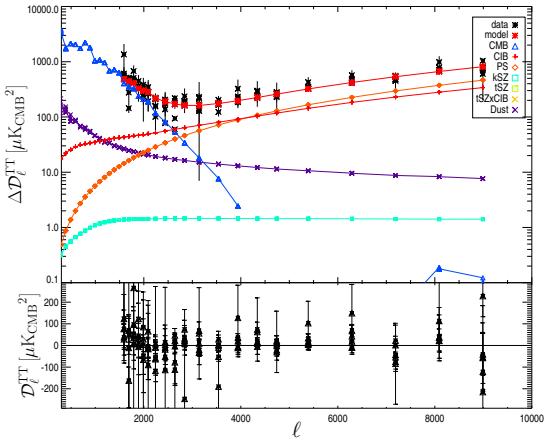

(f) ACT_south 218×218 GHz

Figure C.1. Power spectra of CMB and foregrounds as fitted by the Hillipop+VHL likelihood compared with ACT data. The use of window functions explain why the CMB component sometimes reappears at the very end of the multipole range.

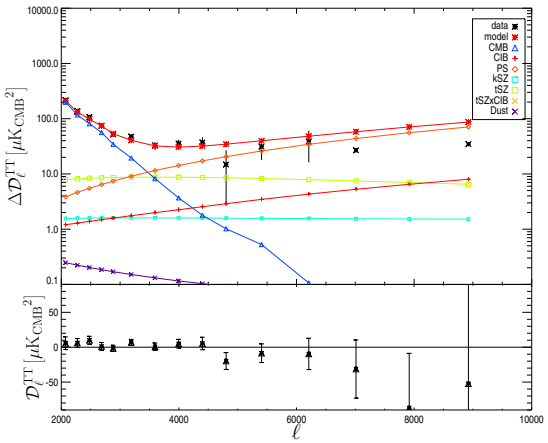

(a) SPT_high 95×95 GHz

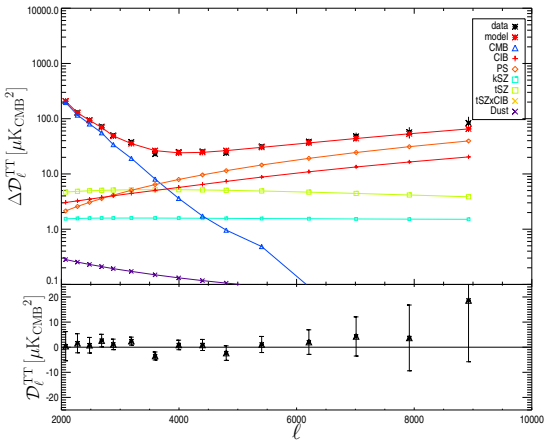

(b) SPT_high 95×150 GHz

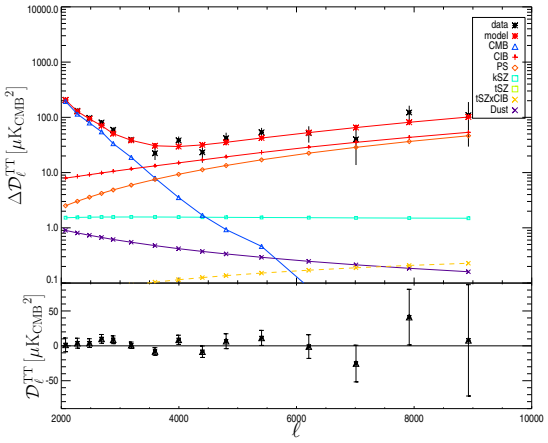

(c) SPT_high 95×220 GHz

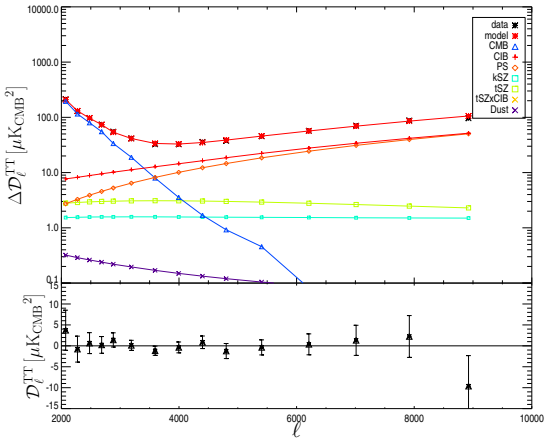

(d) SPT_high 150×150 GHz

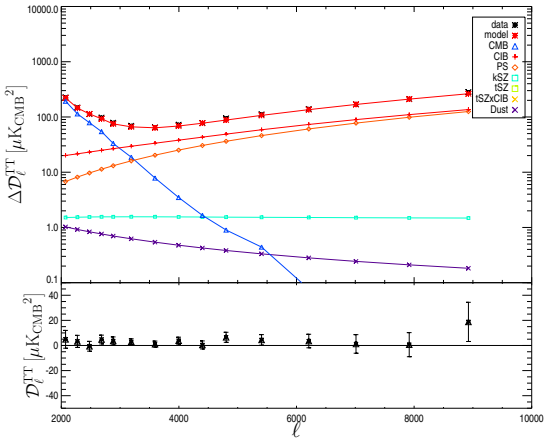

(e) SPT_high 150×220 GHz

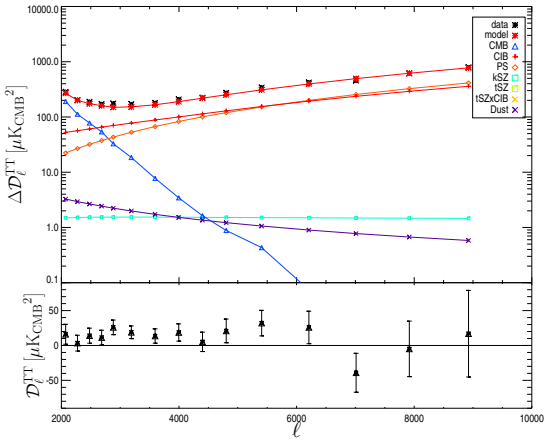

(f) SPT_high 220×220 GHz

Figure C.2. Power spectra of CMB and foregrounds as fitted by the Hillipop+VHL likelihood compared with SPT_high data.

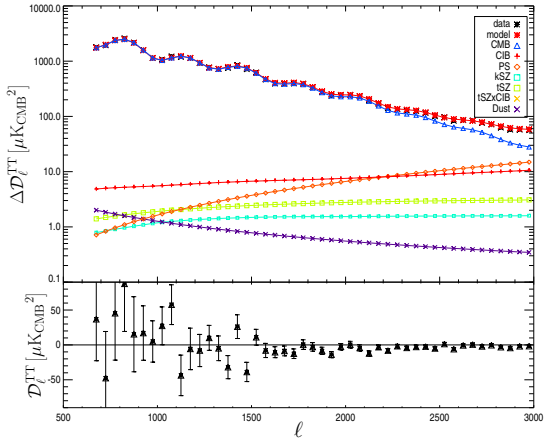

(a) SPT_low 150×150 GHz

Figure C.3. Power spectra of CMB and foregrounds as fitted by the Hillipop+VHL likelihood compared with SPT_low data.